Paper submitted to the International Journal of Robotics Research

Special Issue CLAWAR 2004

Reliable, Built-in, High-Accuracy Force Sensing for Legged Robots

Hector Montes
Technological University of Panama
Apartado Postal 0819-07289
El Dorado, Panama City, Panama
hector.montes1@utp.ac.pa
hector.montes@csic.es

Samir Nabulsi, Manuel A. Armada
Automatic Control Department
Industrial Automation Institute – CSIC
28500 La Poveda, Madrid, Spain
snabulsa@iai.csic.es
armada@iai.csic.es

Abstract

An approach for achieving reliable, built-in, high-accuracy force sensing for legged robots is presented in this paper, based on direct exploitation of the properties of a robot's mechanical structure. The proposed methodology relies on taking account of force-sensing requirements at the robot-design stage, with a view to embedding force-sensing capability within the mechanical structure of the robot itself. The test case is ROBOCLIMBER, a bulky, quadruped climbing and walking machine whose weighty legs enable it to carry out heavy-duty drilling operations. The paper shows that, with finite-element analysis of ROBOCLIMBER's mechanical configuration during the design stage, candidate positions can be selected for the placement of force transducers to measure indirectly the contact forces between the feet and the ground. Force sensors are then installed at the theoretically best positions on the mechanical structure, and several experiments are carried out to calibrate all sensors within their operational range of interest. After calibration, the built-in sensors are subjected to experimental performance evaluation, and the final best sensor option is found. The built-in force-sensing capability thus implemented is subjected to its first test of usability when it is employed to compute the actual centre of gravity of ROBOCLIMBER. The method is shown to be useful for determining variation during a gait (due to the non-negligible weight of the legs). Afterwards the force sensors are shown to be useful for controlling foot-ground interaction, and several illustrative experiments confirm the high sensitivity, reliability and accuracy of the selected approach. Lastly, the built-in sensors are used to measure ground-reaction forces and to compute the zero-moment point for ROBOCLIMBER in real time, both while standing and while executing a dynamically balanced gait.

KEY WORDS – Climbing and walking robots, finite-element analysis, force sensor, foot-ground interaction, force-feedback control, zero-moment point.

1. Introduction

Early industrial applications of robot technology focused on the performance of simple tasks, like parts handling and spot welding, with no use of external sensors. Very soon, however, it became clear that many features of robot performance could be improved by adding some kind of feedback concerning both the task at issue and the performance of that task. So, the increasing demand for improved robot design and performance led to the development of several control strategies using different kinds of sensors. For example, when robot manipulators are meant to work in contact with the environment, then the main control objective is to regulate the force and torque that the manipulator exerts on the environment while (in one well-known classical approach) controlling the position in those directions for which the environment does not impose restrictions. One of the first investigations into force analysis for mechanical hands can be found in (Salisbury and Roth 1983). Other developments related to the measurement of forces at the end effector of a manipulator (e.g., a gripper) can be found in (Gorinevsky et al. 1997; Siciliano and Villani 1999; Spong and Vidyasagar 1989), and yet other findings regarding measurements at different parts of robots (e.g., legs, feet, etc.) can be found in (Gorinevsky and Schneider 1990; Kumar and Waldron 1990; Gardner 1992; Galvez et al. 1998). Good literature reviews have been published as well (Whitney 1987; Grieco et al. 1994).

Nowadays the use of sensors in automation and robotic systems makes it possible for these powerful tools to perform more complex tasks, an option that lends special added value when the environment is less structured and/or partially unknown. Sensors that can measure force, torque, or pressure usually contain an elastic member that translates the mechanical magnitude into a deflection or strain (Dally et al. 1993; Bentley 1995). There is a wide

variety of commercially available sensors that are built on different physical principles for measuring these kinds of signals, e.g., load cells, torque cells, strain gages, etc. Strain gages are employed for the experimental part of this paper, because strain gages are the most common kind of transducer used for force measurement. In these sensors, strain produces a change in the electrical resistance of strain gages mounted on an elastic element. Strain gages engaged as force sensors provide high sensitivity and measurement accuracy and require moderately complex amplifiers. The main drawback to strain gages is their sensitivity to temperature, which has to be neutralized by special methods (Gorinevsky et al. 1997).
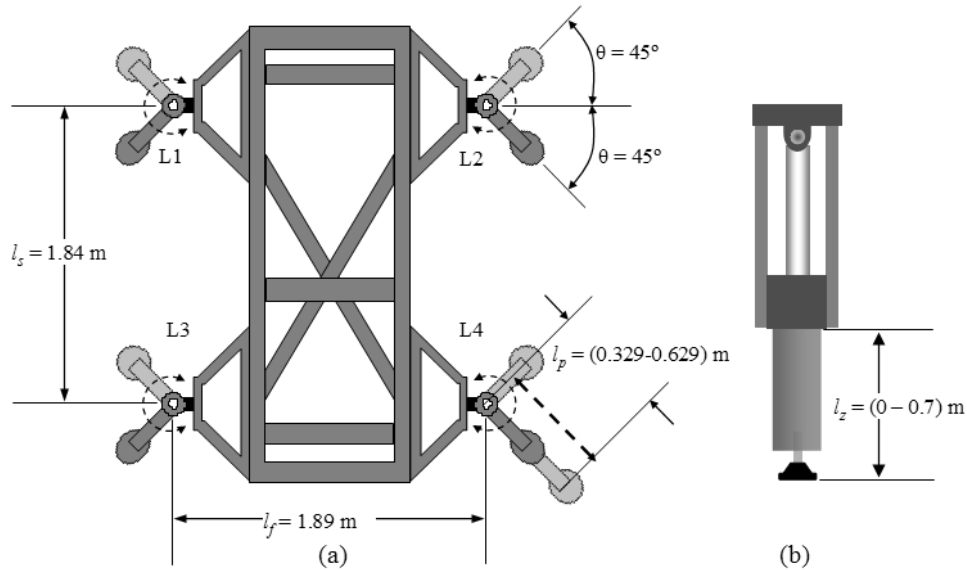
The design (Mosher 1968; Song and Waldron 1988; Pugh et al. 1990; Armada 1991; Arikawa and Hirose 1996; Hirose 1997; Waldron and Kinzel 1999; Waldron 2000; Pfeiffer et al. 2000) and the application of legged robots (climbing and walking) are the subject of widespread, increasing interest to the scientific community (Gonzalez de Santos et al. 1994; Armada and Gonzalez de Santos 1977; Armada et al. 1997; Maza et al. 1997; Armada 2000; Armada et al. 2002; Gonzalez de Santos et al. 2000; Armada et al. 2003; Virk et al. 2004). Legged-robot displacement is characterised by the opening and closing of the robot's various kinematic chains on terrain that yields to multiple foot-ground contacts along a given gait (Estremera and González de Santos 2003), resulting in a changeable pattern of reaction forces that ultimately determines overall machine stability. For this reason, intensive research has been devoted over the last two decades to force-based control in walking robots, and, hence, force sensing is becoming a hot topic in walking-robot control, owing to the obvious advantages that could be obtained by implementing force-feedback control strategies. Force control can be used to optimise walking-robot design, avoid the risk of foot slippage, investigate force distribution, smooth the robot's motion, improve energy efficiency, identify mechanical properties, and subsequently expand robots' operational capabilities (Gorinevsky and Schneider 1990; Galvez et al. 1998; Galvez et al. 2000).

This paper looks at force-sensing strategies in legged robots (Montes 2005). The proposed methodology relies on taking account of force-sensing requirements at the robot-design stage, with a view to embedding force-sensing capability within the mechanical structure of the robot and, in so doing, avoiding the later addition of expensive and/or large commercial sensors (Montes et al. 2004). The test case is ROBOCLIMBER (Acaccia et al. 2000; Armada and Molfino 2002), a bulky, quadruped climbing and walking machine whose weighty legs enable it to carry out heavy-duty drilling operations in the construction industry (Armada and Gonzalez de Santos 2001). A finite-element analysis is conducted of the mechanical structure of the robot's legs. From this study, specific positions are selected as candidates for the location of strain gages for the indirect measurement of the contact forces between the foot and the ground. This will provide the robot with built-in force-sensing capability. Several experiments are then carried out with the built-in force sensors implemented at the theoretically best positions, sensors are calibrated, and the results are experimentally evaluated. As the first application, the built-in force-sensing capability is employed to compute the centre of gravity for ROBOCLIMBER, where the development demonstrates its usefulness for determining COG variation during a gait (due to the non-negligible weight of the legs). Additionally, a simple velocity-control scheme using force feedback is employed for controlling foot-soil interaction for soils with different stiffness properties. Lastly, in the final part of the paper, built-in force sensors are used to measure ground-reaction forces and to compute the zero-moment point (ZMP) for ROBOCLIMBER in real time, both while standing, in order to ascertain the point where the reaction force of the ground acts, and while executing a dynamically balanced gait, to determine if the ZMP lies inside the support polygon and to enable the performance of stable gaits with compliance movements (Montes et al. 2004a).

2. General configuration of ROBOCLIMBER

ROBOCLIMBER (Acaccia et al. 2000; Armada and Molfino 2002; Anthoine et al. 2003) is a quadruped walking and climbing robot of large dimensions whose development was funded by the EC under a Growth/Craft project, where the objective was to develop a tele-operated service robotic system to perform consolidation and monitoring tasks on rocky slopes. The robot's entire concept is based on a mechanical structure (Molfino et al. 2005) with a total mass of about 1973 kg. The legs have a cylindrical configuration. Each leg of the robot has three degrees of freedom, one rotation joint and two prismatic joints (horizontal and vertical), and the total mass of one leg is about 170 kg. The system is designed to overcome obstacles somewhat greater than 500 mm. Robot legs are designed so that they are very tough and no practical bending is allowed (by manufacturing) especially for the third prismatic joints, and so the machine very stiff in the plane orthogonal to these joints.

The mechanical configuration of the robot is shown in Figure 1. In Figure 1a, the four rotational joints and the four prismatic radial joints can be observed. The rotational joints have a stroke of ±45º, and the prismatic radial joints have a displacement of 300 mm and a maximum extension of 629 mm. The third joint (the vertical joint, see Figure 1b) has a prismatic displacement of 700 mm. The distance between any two adjacent joints from the front view is $l_f = 1.89$ m, and from the lateral view, $l_s = 1.84$ m (see also Figure 1c).

$\theta = 45°$

$\theta = 45°$

L1   L2

L3   L4

$l_s = 1.84$ m

$l_p = (0.329\text{-}0.629)$ m

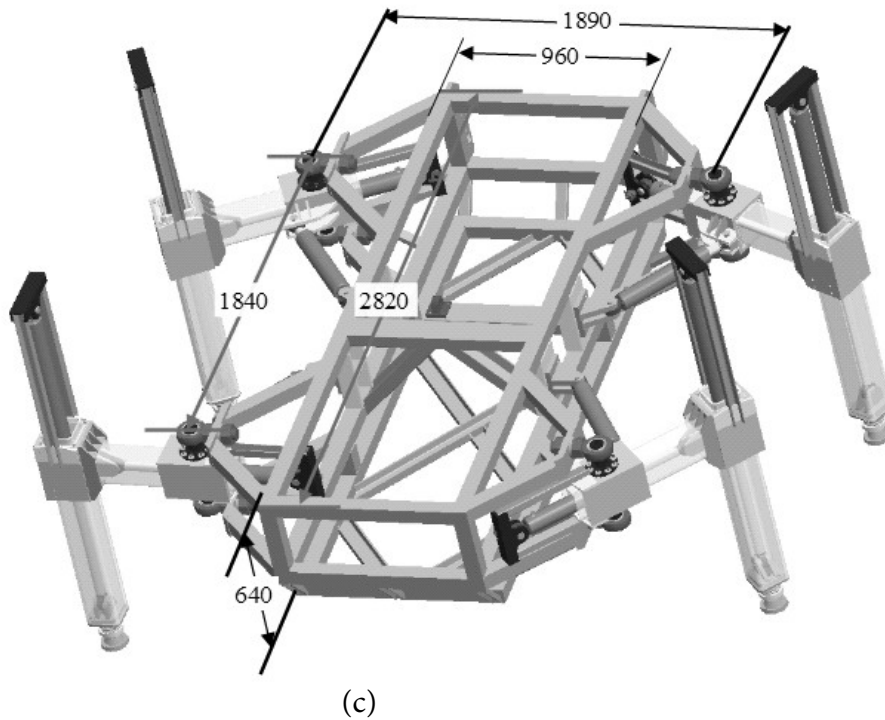$l_z = (0 - 0.7)$ m

$l_f = 1.89$ m

(a)

(b)

(c)

Fig.1. Kinematic parameters of ROBOCLIMBER; (a) Top view of the robot; (b) lateral view of one leg; (c) 3D view showing main dimensions (in mm.).

ROBOCLIMBER axes are driven by hydraulic cylinders and are controlled by means of proportional valves. Hydraulic power unit (16 Kw), drilling equipment (an extra load of about 1500 kg), control system (Nabulsi et al. 2003; Nabulsi et al. 2004), and other auxiliary elements to perform mountain-slope consolidation and monitoring tasks are carried on-board. The robot is supervised from a remote location with no need of operators on board (Steinicke et al. 2004).

ROBOCLIMBER works by climbing uneven mountain slopes with inclinations ranging from 30º to almost 90º. To do so, and because there is no special grasping devices to hold the robot feet on the slope, ROBOCLIMBER has to be held by two steel ropes secured at the top of the mountain and helped to pull itself up by two special hydraulically driven devices called rope tensioning appliance installed on board (a good report was released by the Discovery Channel (Discovery Channel 2005)). The robot's body displacement and the pulling force must be controlled simultaneously for proper climbing (Nabulsi and Armada 2004). This is a major difference with other free climbing robots (Grieco et al. 1998), which use several kinds of adhesion devices (magnets, suction cups, etc.). In this way, shear forces on the robot feet are minimised (although of course they exist) and the operational requirements are placed on the vertical third robot joints. Moreover, one of the ROBOCLIMBER tasks is to perform heavy duty drilling in a direction orthogonal to the ground, and so in the same direction that the third prismatic joint of the robot. Reaction forces in the orthogonal direction to the slope are expected during drilling and during removing the drilling rods from the rocky slope. Also, the uneven surface requires using the third joints of the legs to adjust the drilling unit as close as possible to 90º against the slope. This leads to consider first force sensing in this direction. The working situation for ROBOCLIMBER is illustrated in Figure 2, which should not be misunderstood and only serves to the purpose of showing some of the main acting forces.
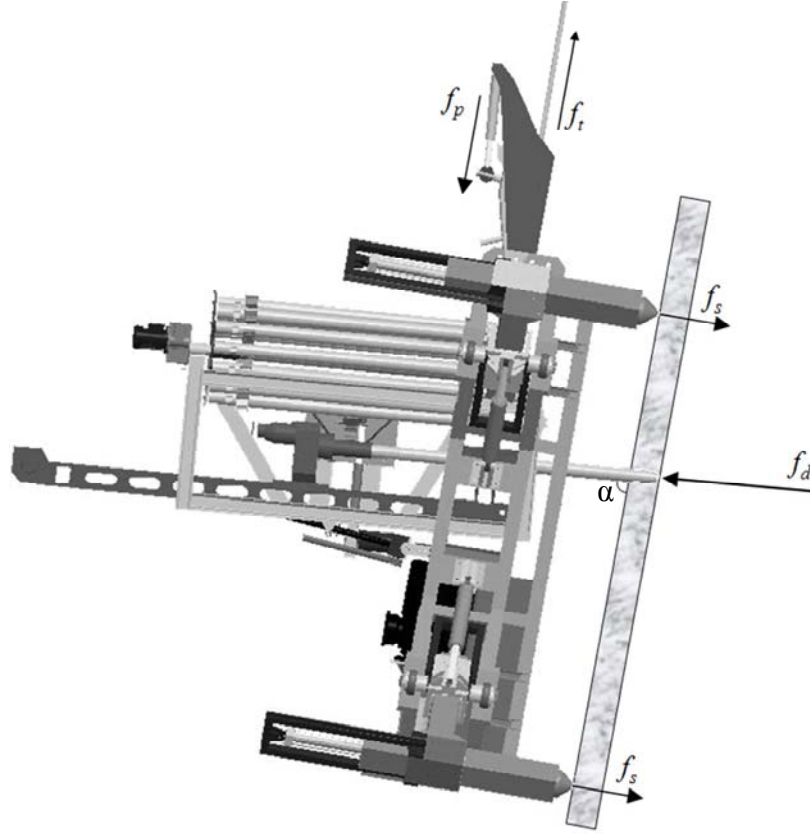
Fig.2. ROBOCLIMBER working on a slope. Only some acting forces are shown: f_t: tensioning force; f_p: propulsion force; f_s: support force; f_d: drilling force. ROBOCLIMBER design courtesy of PMARLab (University of Genoa).

During static equilibrium it can be assumed that $f_t = f_p$, and then low forces (compared with f_t) could be expected in the feet in the slope direction if proper traction is provided. Drilling force f_d can be positive or negative, as it was commented above. So, it becomes interesting to measure the forces in the third joint of the legs while the machine is performing drilling tasks because the support forces (f_s), made only by the weight of the robot, can be surpassed by the drilling forces (f_d) while penetrating the surface (the robot will tend to detach from the wall) or increased dramatically while removing the drilling rods (the robot will tend to grasp the wall). Doing so, it will be possible to help control the drilling process (rotation speed and pushing force of the drilling unit) and to increase process performance.

By other side, mountain slope is uneven and the legs need to be instrumented to properly keep contact with the supporting surface. To detect contact of feet and ground the feet are equipped with on-off sensors. However, this is not enough when drilling because there are many vibrations and the on-off signals lead to poor stability and oscillations of the robot. In conclusion, there are several reasons to sense force in the drilling direction. Figure 3 shows ROBOCLIMBER field tests.

Fig. 3. ROBOCLIMBER field tests: a) Climbing: Alps, Northern Italy; b) Walking: Industrial Automation Institute (IAI-CSIC) outdoor facilities.

3. Implementing built-in force sensing in a legged robot

When the legs of the robot contact the ground, the force sensors embedded in each leg must be able to detect the contact and measure the force magnitude; and so it should be possible, for example, to calculate the robot's centre of pressure in real time. Control strategies could then be implemented to keep the centre of pressure inside the support polygon of the robot. This has obvious implications for achieving better stability control. Moreover, many other possibilities are then opened, and the applicability of several force-feedback control strategies could be investigated (Hogan 1985; Whitney 1987; Fisher and Mujtaba 1992; Gardner 1992; De Schutter et al. 1998; Chiaverini and Siciliano 1999; Carelli at al. 2004).

In order to provide ROBOCLIMBER with force-sensing capabilities, a finite-element analysis (FEA) was first run, using the Pro/Mechanica modulus of Pro-Engineer® software. The strain was calculated when several loads were applied to the robot leg. After the FEA was performed, several possible target locations were selected for force measurement using the elastic-deformation properties of the leg material. The best locations were the top of the leg structure, one of the sides of the leg structure, and the support axis of the foot. These three locations were good candidates to instrument. Although lateral bars are "transmitting" half of the total force (Figure 4a), depending on their configuration and material it could be possible (from the FEA) to use them (theoretical deformation was enough). Figure 4 shows a scheme of force distribution in the leg, and one example of these FEA analyses with 7500 N of applied force. On the other hand, as it was anticipated in previous sections, the robot is hold up by two steel cables from the top of the mountain. When climbing, cable tension holds the robot, and shear forces on the robot foot are assumed to be small. For this reason lateral loading is assumed negligible for our purposes. In case that off-leg-axis loads could influence on the force measurement, it will be more noticeable in the foot axis and then in the lateral

bars, even if the strain gages are placed to work only in tension/compression. Influence of lateral loads will be obviously smaller for the gages located in the top of the leg, and this is another reason to consider it as a good option.
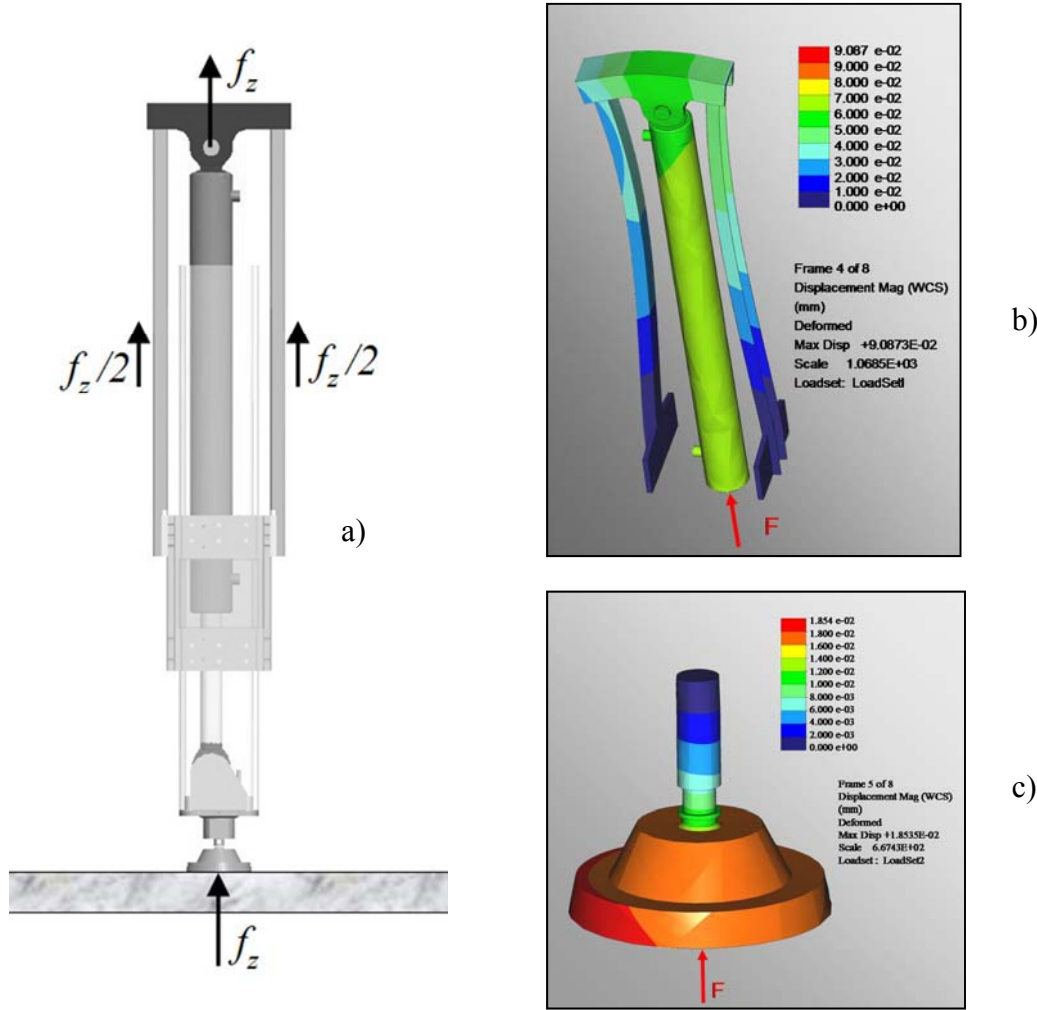

Fig. 4. Force analysis on the leg of ROBOCLIMBER: a) Scheme of force distribution; b) FEA on the leg structure; and, c) FEA on the foot.

Even though being very reliable, FEA analysis needs to be confirmed in practice, because there are many factors that cannot be thoroughly simulated. Moreover, changes in type of material, dimensions and section shape of piece could allow or not to get reliable measurements in the range of interest. Also bridge configuration depends on those features. Accordingly, three force sensors were implemented on each leg, as it is shown in Figure 5.
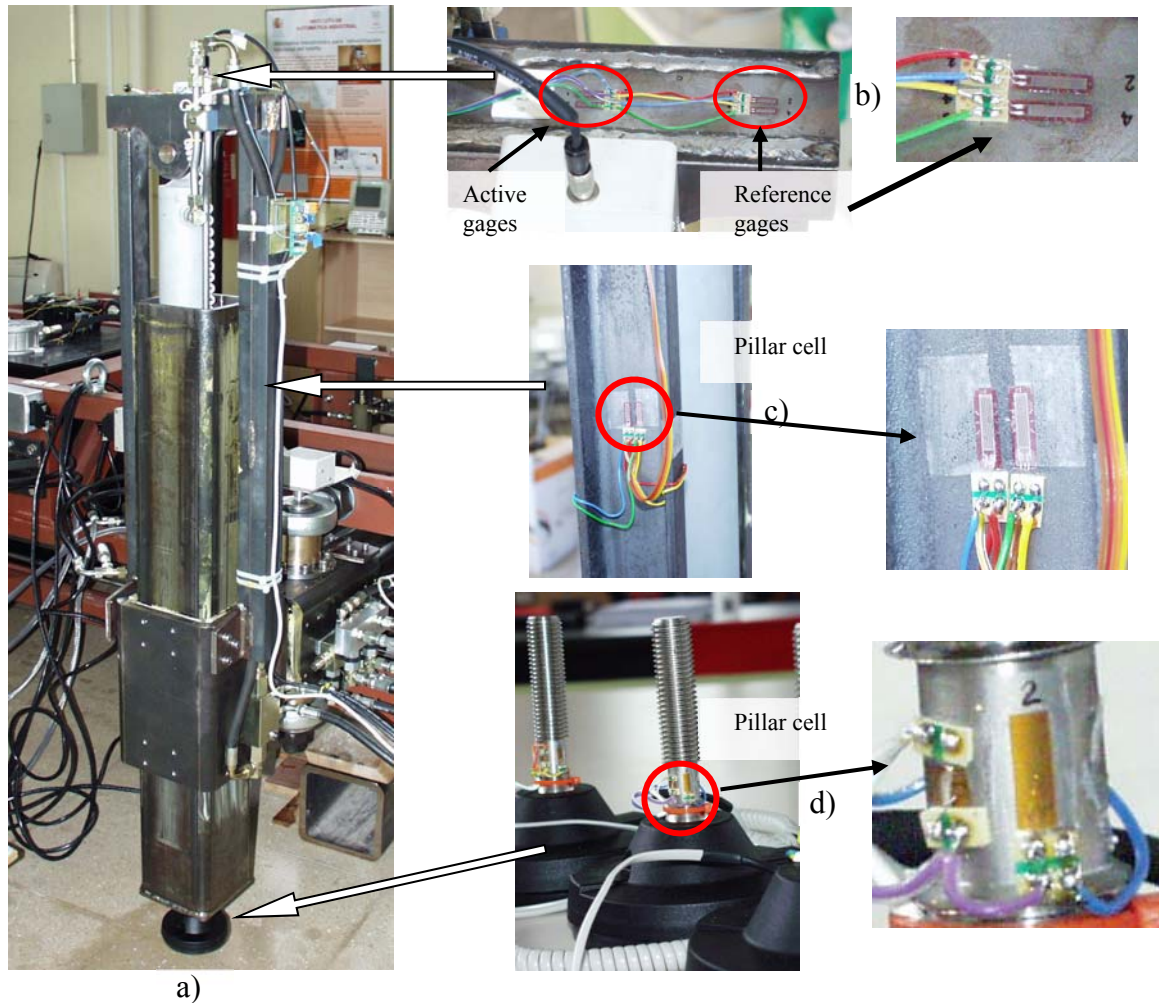
Fig. 5. (a) ROBOCLIMBER's leg made of steel of different kinds; (b) force sensor at the top of the leg; (c) force sensor on the side beam of the leg; and (d) force sensor on the support axis of the foot.

Top sensing is obtained using the principle of a beam that is deformed near the middle, and this deformation can be reliable obtained with a half bridge. Deformation of the beam can be very sensitive (it depends on material and dimensions). .Foot axis is like a pillar and it is better to use a full bridge. Tension/compression of the foot axis depends heavily on the axis diameter and material.

Strain gages were placed in a Wheatstone full-bridge configuration. For the strain gages at the top of the leg, the configuration actually operated like a half bridge, because two of the gages behaved as reference resistances. The reference strain gages were placed on an unstrained zone, while the other strain gages were affixed to the theoretically most strained area, which was found from the finite-element analyses, conducted earlier (Figure 5b).

The second sector where strain gages were adhered was one of the lateral bars of the leg (Figure 5c). This region was initially considered less sensitive to the deformations caused by the reaction forces of the leg against the ground (Figure 4). Several experiments were run to measure the contact forces of the leg with the ground, but the results were not enough satisfactory. For this reason, this sensor was disregarded.

Finally, another force sensor was installed on each axis of the robot foot, in a Wheatstone full-bridge configuration (Figure 5d). The goal was to obtain force measurements throughout the foot bar; therefore, this sensor was expected to behave as if it were a single-axis load cell.

3.1 Calibration procedure

The force sensors installed on ROBOCLIMBER's legs were calibrated with a reference instrument whose characteristics are shown in Table I. Several runs of calibration tests were performed for each leg of the robot in different working conditions.

In each case, the instrument was placed under the leg whose force sensor was to be calibrated, and position control was used to actuate the hydraulic vertical cylinder, moving the leg downwards in 5-mm increments until a steady measurement was obtained from the reference instrument and from the voltage generated by the force sensor. The output voltage of the strain-gage bridge was found by means of a modular instrumentation amplifier (Montes et al. 2004a). These data were recorded in real time by a data-acquisition system.

Table I. Reference instrument-characteristics

Maximal measurement	Scale	Standard deviation	Uncertainty
3000 Kg.	1 Kg.	0.1722 Kg.	0.5992 Kg.

The calibration process consists in calculating a diagonal matrix representing the relationship between the electrical voltage measured at each of the force sensors on the robot's legs and the forces measured by the reference instrument. The function is expressed as: $F = (1/v_s) Kv + b$, where K is a diagonal matrix, v is the voltage-vector differences measured by the sensor matrix, b is a constant matrix, and v_s is the voltage of the power supply feeding the Wheatstone bridge. For the sensor at the top of the leg, the resulting equation is given by,

$$\begin{bmatrix} F1 \\ F2 \\ F3 \\ F4 \end{bmatrix} = \frac{1}{v_s} diag. \begin{bmatrix} 87475 & 79598 & 82335 & 151113 \end{bmatrix} \begin{bmatrix} v_{def1} - v_{ud1} \\ v_{def2} - v_{ud2} \\ v_{def3} - v_{ud3} \\ v_{def4} - v_{ud4} \end{bmatrix} + \begin{bmatrix} 3413 \\ 4344 \\ 4803 \\ 8410 \end{bmatrix} \qquad (1)$$

For the sensor on the support axis of the foot of the robot, the forces are given by,

$$\begin{bmatrix} F1 \\ F2 \\ F3 \\ F4 \end{bmatrix} = \frac{1}{v_s} diag. \begin{bmatrix} 28651 & 20868 & 23978 & 20463 \end{bmatrix} \begin{bmatrix} v_{def1} - v_{ud1} \\ v_{def2} - v_{ud2} \\ v_{def3} - v_{ud3} \\ v_{def4} - v_{ud4} \end{bmatrix} + \begin{bmatrix} 16.1 \\ 30.0 \\ -33.1 \\ 87.1 \end{bmatrix} \qquad (2)$$

where v_{def} is the voltage measured by the strain gages deformed when a force is applied to the leg and v_{ud} is the voltage of the strain gages when no forces are applied.

Interestingly, each strain gage's Wheatstone bridge proved especially sensitive to certain forces, depending on its location on the mechanical structure of the robot. The coefficients shown in equations (1) and (2) were systematically verified by measuring known forces at many different positions of the robot's legs along the Z axis.

Figure 6 shows the calibration result of the force sensors built into each leg of the robot. As mentioned above, only the results of the sensor at the top of the leg and the sensor embedded in the support axis of each foot are shown in this figure. The sensors display approximately linear performance, and the sensors located on the feet prove themselves to be more sensitive than those installed at the top of the leg. Also, note that the sensitivity of the force sensor placed on the foot bar is (in some cases) up to 15 times greater than that of the sensor placed at the top of the leg.
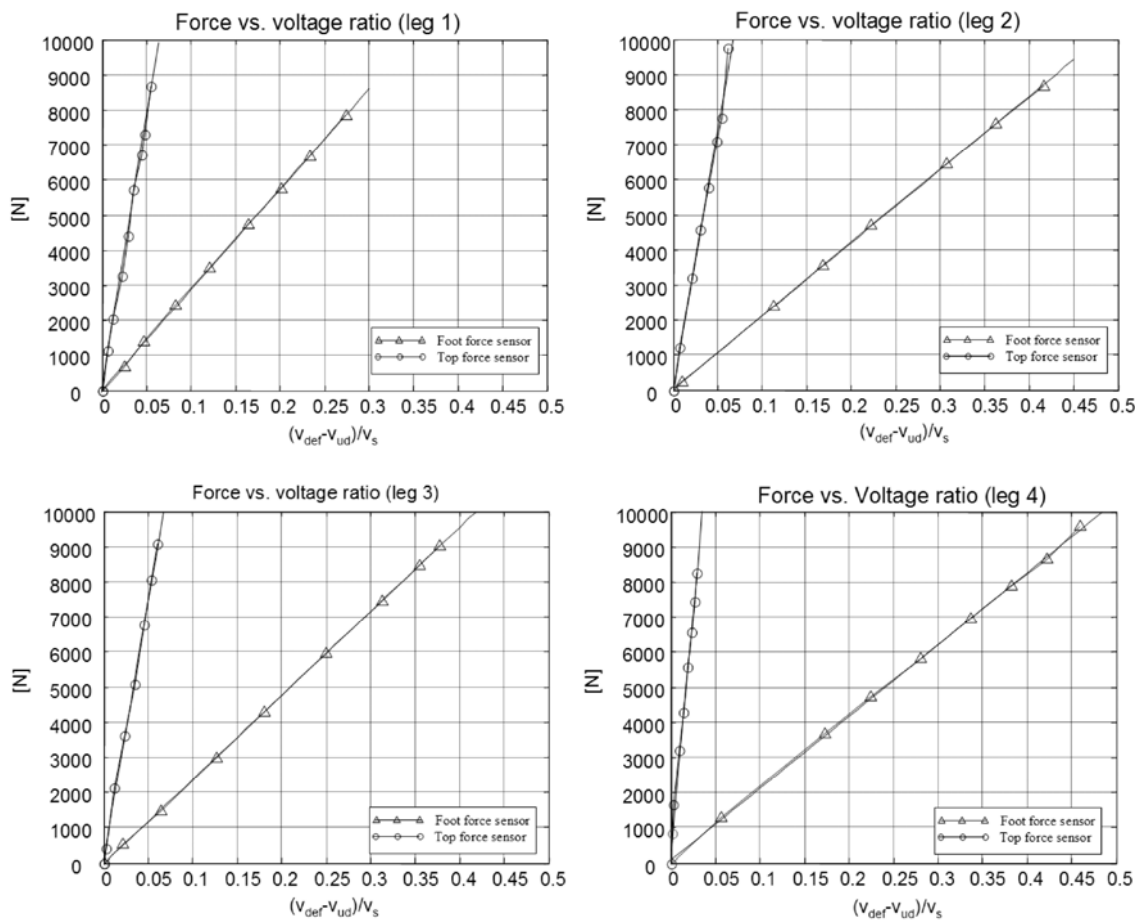

Fig. 6. Calibration results and comparison between two different force-sensor configurations.

In conclusion, experimentation yielded to discard the lateral bars, although modification of their section could eventually enhance the result. By other side we tried in principle to avoid instrument foot axis because this is a "harsh" place for several reasons: it is subject to shocks (and so to large stress) and vibrations, it requires longer cabling, and the signal transmission could get undesirable noise in its way from the foot to the instrumentation amplifier. Also, for climbing and drilling a robust foot is required, and then its diameter needs to be increased leading to less sensitivity. So, top sensing was the best option by practical reasons. The major advantage of the top measurement is that this place is the best in practice (it is far from

dangerous area and easier to instrument and to connect and repair). The main advantage of legdown is its promptness for walking tests in lab. Nevertheless, legtop and legdown bridges can be used in practice, being the main difference their sensitivity. In this situation of trade-off both sensing strategies are subject of experimental evaluation in next section.

4. Experimental evaluation of built-in force sensors

Several experiments were conducted using ROBOCLIMBER's built-in force sensors, in which measurements were taken of the reaction forces of the legs. These force measurements were made in two different sectors of each robot leg, where the force sensors were installed: on the upper part of the leg structure and on the support axis of the foot. Some experimental results are shown in Figure 7 and Figure 8, which display the force on each leg and the resultant force obtained with both sensor configurations.

The test sequence that was used in the first experiment (to evaluate the legtop force sensor) consisted in raising the robot 0.5 m from the ground, starting from a position where all the legs were not in contact with the ground, i.e., the frame of the robot was on the ground. Transient phenomena were observed until the forces stabilized at their steady values, due to the force-distribution problem in a four-legged robot and the hysteresis posed by the material where the strain gages were installed.
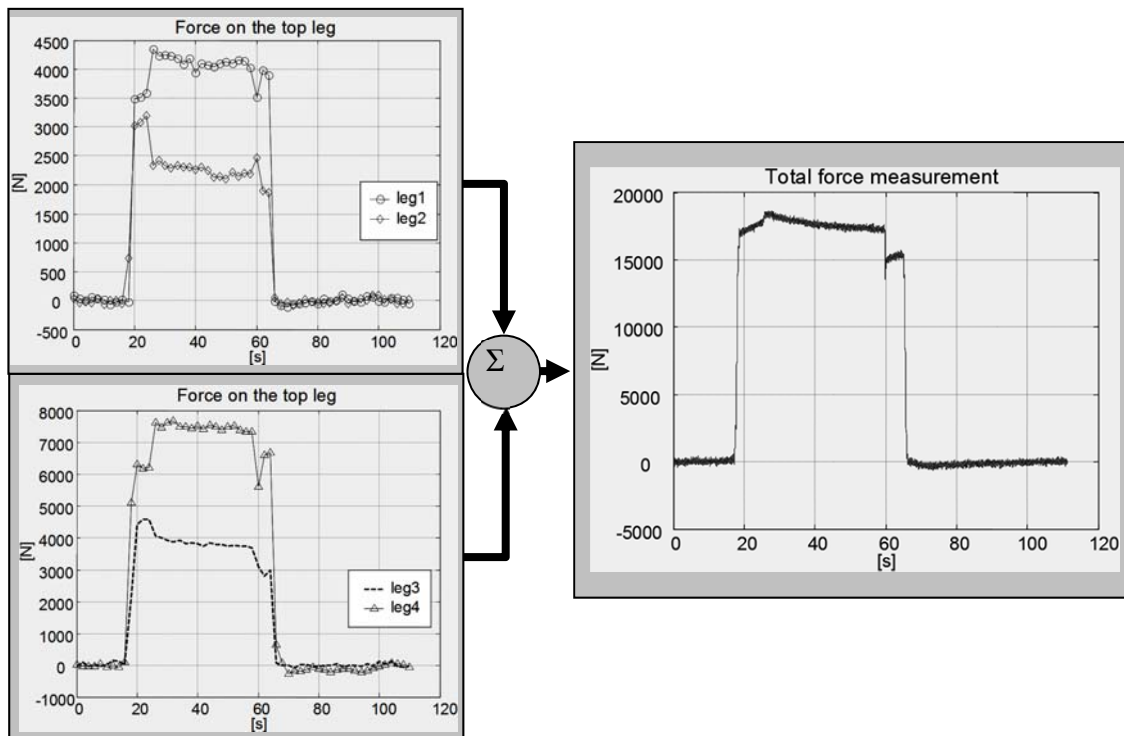

Fig. 7. Force measurement with the leg top sensors.

In this experiment, the robot remained on its feet for approximately 50 seconds. It took approximately 7 seconds from the first moment when one of the legs touched the ground until the robot stopped rising, having reached the height defined in the strategy. At this time a force-distribution phenomenon took place, because each leg was in fact moving at different

velocities, which explained any slight oscillation of the robot body. When the legs lifted the robot, the hysteresis characteristic took place. At this point, the steel plate where the strain gages were pasted began to return to its natural state, after the deformation tolerated at the beginning of the process. The forces became stabilized 50 seconds after the legs made contact with the ground, and at this moment (second 60) the total measured force was 17700 N (mass of 1804 kg), which represented a relative error of 8.56% with respect to the real weight (mass of 1973 kg). Furthermore, the transient could also be observed when the robot initiated its downward movement.
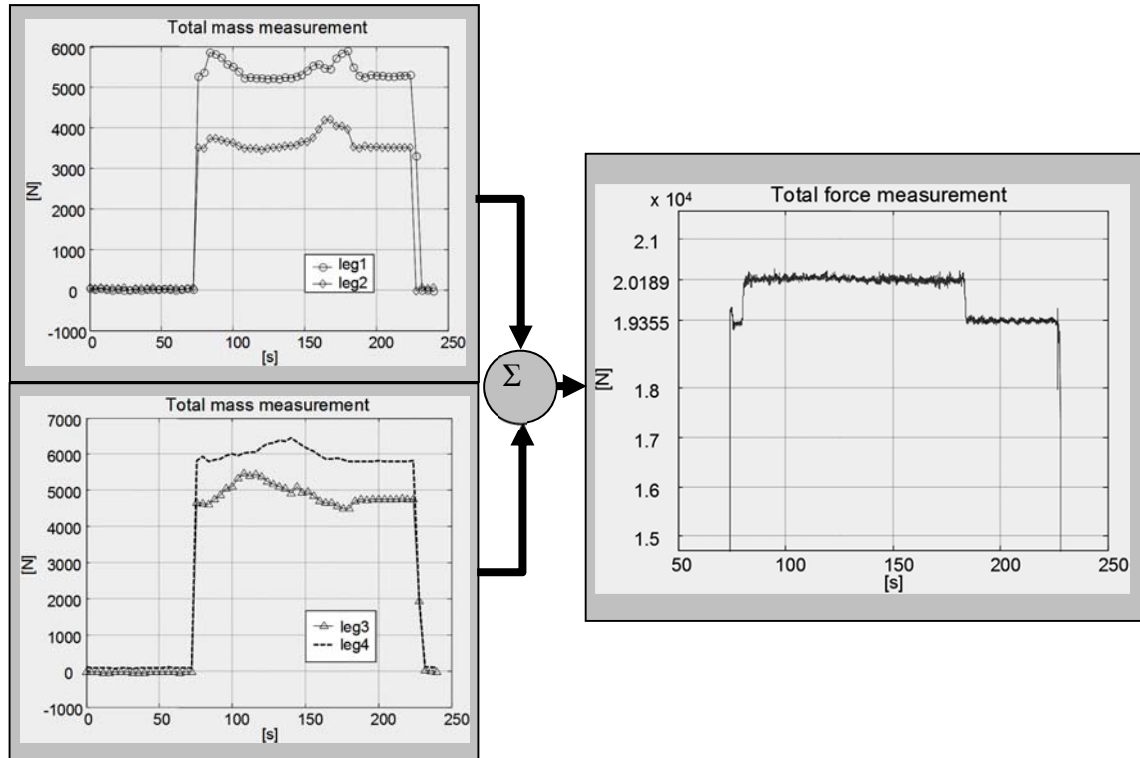

Fig. 8. Force measurement with the sensors on the support axis of the foot.

With the second force-sensor implementation (sensor on the foot bar), the robot rose 0.50 m from the ground and remained on its feet for approximately 150 seconds (see Figure 8). In this experiment, an external disturbance was added that consisted in the displacement of a mass of 85 kg (834 N) on top of the robot structure. The mass displacement began at time t ≈ 80 sec and lasted until t ≈ 180 sec. In this case, the average force measurement was 19320 N (1969 kg) when the robot remained on its feet without the extra mass on top; when the object was added, the average force measurement was 20110 N (2050 kg) during the time the mass remained on top of the robot structure. In spite of the fact that the total force measurement was almost constant in both steps, the variability of the force measurement in each leg caused by the object travelling on top of the robot was apparent.

Nevertheless, the relative error calculated in both measurements for the second force-sensor implementation, with or without the disturbance, is 0.5% in the worst of cases. This result indicates the high accuracy and reliability of the built-in force sensor implemented in this robot. The transient phenomenon takes place when a leg makes contact with the floor and in the instant when the robot begins the process of descent. The hysteresis phenomenon was not observed in this experiment, although it was detected in the preceding experiment. The

conclusion drawn from its absence is that force sensors embedded on the support axis of each foot are a very important improvement over force sensors placed at the top of the robot's leg structure. For this reason, although the leg top sensor is easier to implement and use, the foot sensor is employed henceforth because it outperforms the leg top version.

To end our evaluation of built-in force sensors, we will use the sensors to locate ROBOCLIMBER's centre of gravity and show that there is a non-negligible variation of the robot's COG during a gait, which should be taken into account when using this legged robot. Frequently, in a great deal of work on walking robots, it is assumed that the centre of gravity is located at the geometric centre of the robot's body. In such cases, it is assumed that the robot's mass is uniformly distributed and the weight of the legs is negligible. For a lightweight robot such assumptions may be feasible, because the measurement error is not very significant, but for a large robot where each leg accounts for 8% of the robot's total mass and several pieces of equipment are distributed on board, as in the case of ROBOCLIMBER, such an assumption will not necessarily be valid.

We therefore carried out an interesting, simple experiment (albeit a tedious one because of the large number of measurements taken) to locate the centre of gravity. The robot was placed in symmetric postures where the geometric centre of the body is the geometric centre of the posture (see Figure 9).
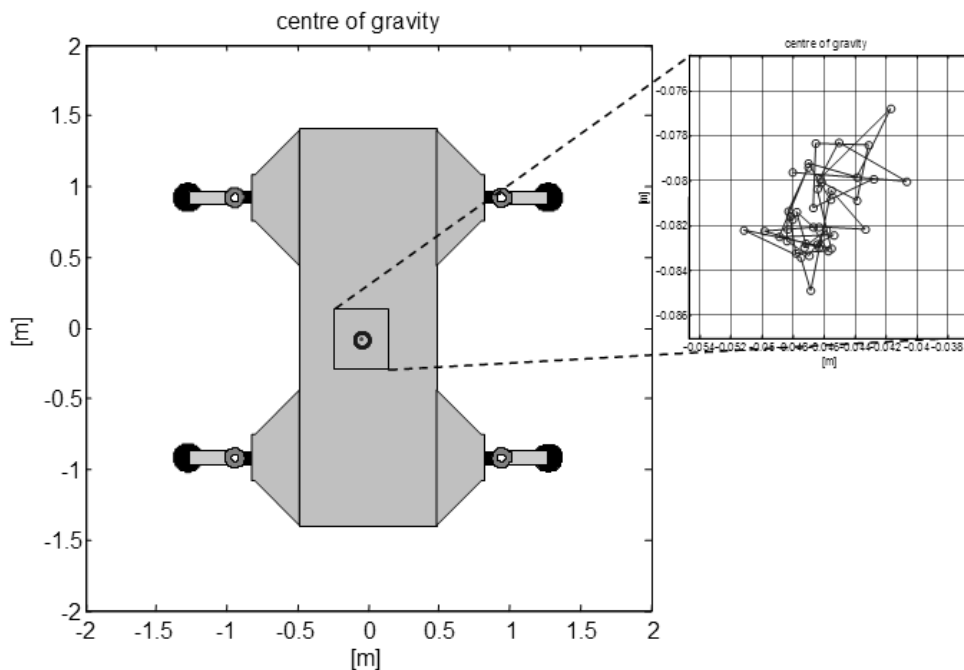

Fig. 9. Centre of gravity of ROBOCLIMBER.

The centre of gravity of the robot (a robot weighing 19730 N in its simplest configuration) was calculated as $\text{cog}_{transversal}$ = -0.0464 m in the transversal plane and $\text{cog}_{sagittal}$ = - 0.0813 m in the sagittal plane. The least-square method was used. The inset in Fig. 9 shows the measurements taken.

The next step is to determine if the centre of gravity changes when the robot performed a gait. Because the legs have considerable mass, the displacement of the robot's centre of gravity should be unavoidably influenced whenever a leg is in transfer phase. Under this hypothesis,

the robot could have a tendency to execute roll and pitch movements at the time that the support polygon is formed by three angles (one leg in transfer).

In order to verify this hypothesis, a gait was performed very slowly, and the position of the centre of gravity was recorded in real time. Figure 10 shows the results of this experiment, verifying that there is a noticeable displacement of ROBOCLIMBER's centre of gravity during the two-phase discontinuous gait. Greater variation appears in the sagittal plane that in the transversal plane. So, the robot may be deduced to have a tendency to pitch during the locomotion, while its roll tendency was practically imperceptible. This does not mean that the robot in fact executes a pitch (because the front leg in support will avoid that), but indicates that a torque is formed aiming to produce a pitch. This effect, added to the natural propensity of the robot body to bend (what is very common in four-legged walking robots when one leg is raised), could lead to increase the low down of the robot body at each step. Tracking COG displacement during locomotion gaits is obviously of great importance in order to modify control algorithms and guarantee robot stability.
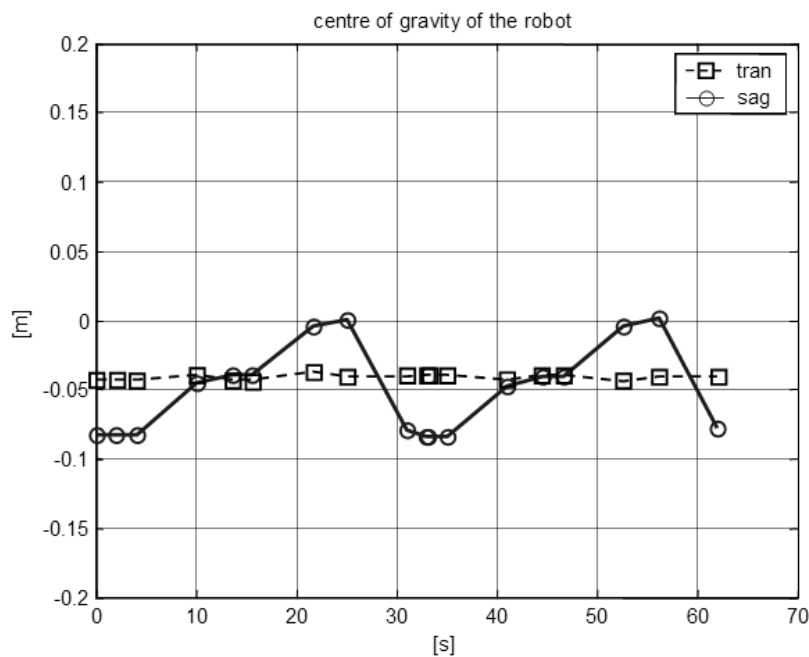

Fig. 10. Using force sensors to find how ROBOCLIMBER's centre of gravity changes during a gait cycle.

5. Controlling foot-ground interaction

Could the proposed built-in force-sensing capability implemented in ROBOCLIMBER be useful in practice for control purposes? As similar developments usually do, ROBOCLIMBER initially uses a basic algorithm for locomotion purposes (two-phase discontinuous gait). When the quadruped robot is moving over uneven terrain (variations of significant height), the execution of this gait forces the robot body to modify its orientation constantly, making it impossible to control robot posture (Gonzalez de Santos and Jimenez 1995). This can eventually cause the robot to tip over. Simply detecting the leg's contact with the ground can suffice to modify the gait slightly, so that the robot adapts to the irregularities of the terrain. This control strategy enables the robot to walk over uneven terrain while maintaining a statically balanced posture.
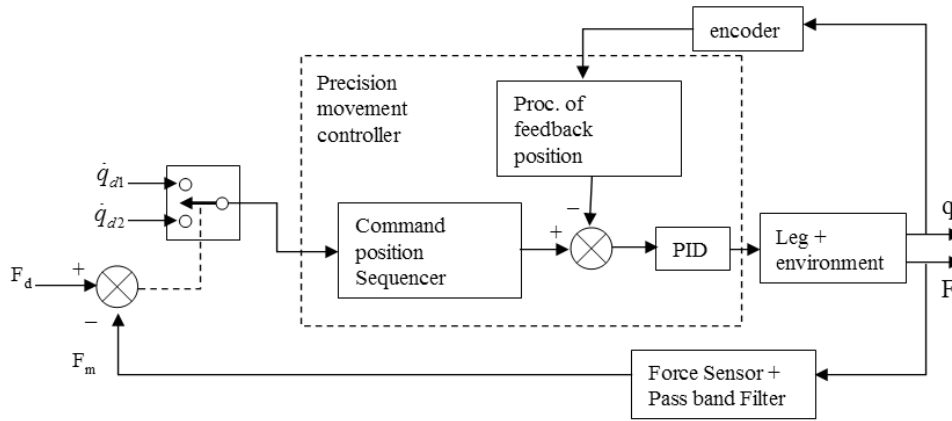
Fig. 11. Controlling foot-ground interaction using simple force feedback.

Obviously, detecting foot-ground contact can be accomplished using simpler means, such as a micro-switch. However, use of such simple sensors is limited to contact detection alone and fails to provide any information about how (with what force) the foot-ground interaction occurs. Moreover, if we wish to know the precise force of interaction, we can use a commercial force sensor (Galvez et al. 2000), but, while this is a good option that comes in a range of prices, it is not always easy to find a sensor that suits the particular requirements of a given robot. This is why this paper proposes taking advantage of the robot's own structural properties to house embedded sensors. This approach is not overly complex, and, as we have shown, it can lead to good results. In any case, the advantages of using force feedback for controlling legged robots are widely recognised (Gorinevsky and Schneider 1990).

Our next experiments follow the scheme shown in Figure 11, which presents a simple force-feedback control system. The goal is to find the fastest way to detect foot contact with the ground at different heights by means of reading the force provided by the sensor. When contact is detected between the foot support and the ground with a measured force F_m which is equal to or greater than a desired force F_d, the control system will change gear to put the leg in reverse. Obviously this is not the best possible control, but it is a simple way of testing the sensors and the speed with which they can be used).

As shown in section 3.1, the built-in foot sensors were, remarkably, very linear over a wide range, from a few N to more than 10000 N. For the experiments, the minimum desired force for ground/object detection was set at 50 N, and many experiments were conducted successfully with different desired force commands. However, during some experiments where the desired force command was less than 50 N, errors were observed in the execution of the strategy. This was because the ripple of the measured force signal, which was produced by the thermal noise in the strain gages and the hysteresis factor of the leg material (after a long period of experimentation), exceeded the desired force command. In any case, force-command values of under 50 N need not be used, because the weight of the robot is near 20000 N, so while the force supported by the legs does vary with the robot's posture during locomotion, the force is always much greater than 50 N. For example, when a desired force command of over 200 N is set, ground detection is almost immediate, because the force sensor is working in a region where the signal-to-noise ratio is very favourable.

Figure 12 shows the results when detecting obstacles at several heights. The strategy was to control the commutation of the velocity commands of prismatic joint 'z' in leg 2 when the detected force reached its set point. For this experiment, the force set point was 150 N (or greater).
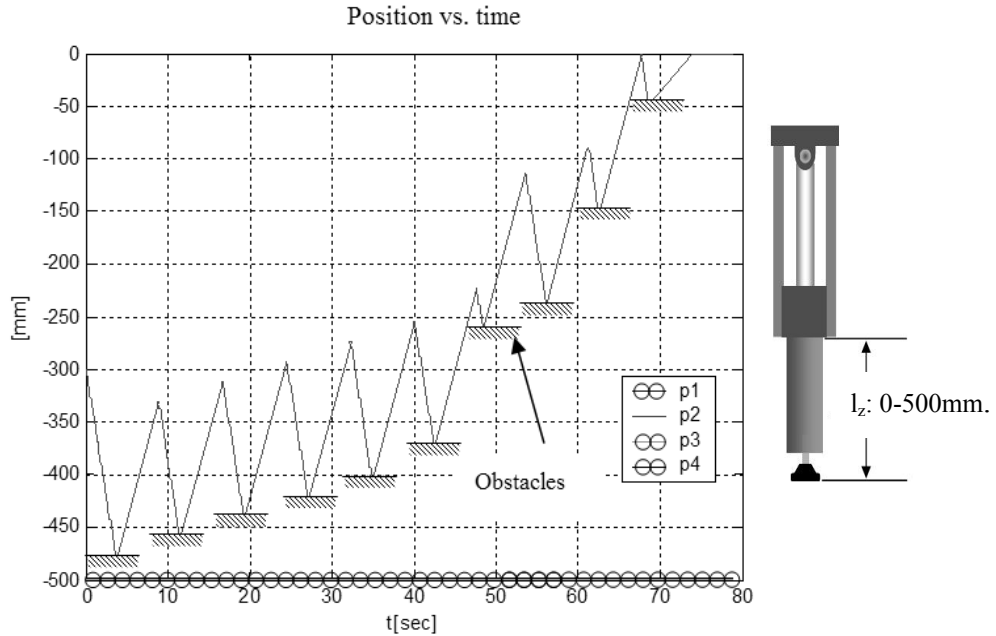

Fig. 12. Force-controlled detection of ground at different heights. In this experiment, leg length ranged from 0 (retracted) to 500 mm (less than maximum possible extension). The force set point was 150 N.

Figure 13 shows contact forces and speeds. The commanded velocity commutation is 30 mm/sec when the leg moves upwards (after detecting the obstacle) and -50 mm/sec when the leg moves downwards (to detect the obstacle). The noise observed in the velocity graph when the leg moves downwards is caused by the vibration of the hydraulic system that powers the leg. This is reflected in small errors of the incremental optical encoder that closes the position loop.

Different force-measurement levels are observed in the force diagram (see Figure 13a). This is because after time=42 sec there are "soft" ground. A "soft" ground absorbs at the start the reaction energy when a leg makes contact with it, which means the force detected is small compared to the force when the leg makes contact with a "hard" ground. For that reason, the commutation time is smaller when soils of greater stiffness are employed. Therefore, the contact-force control accommodates itself to the force command established in the algorithm.

-17-

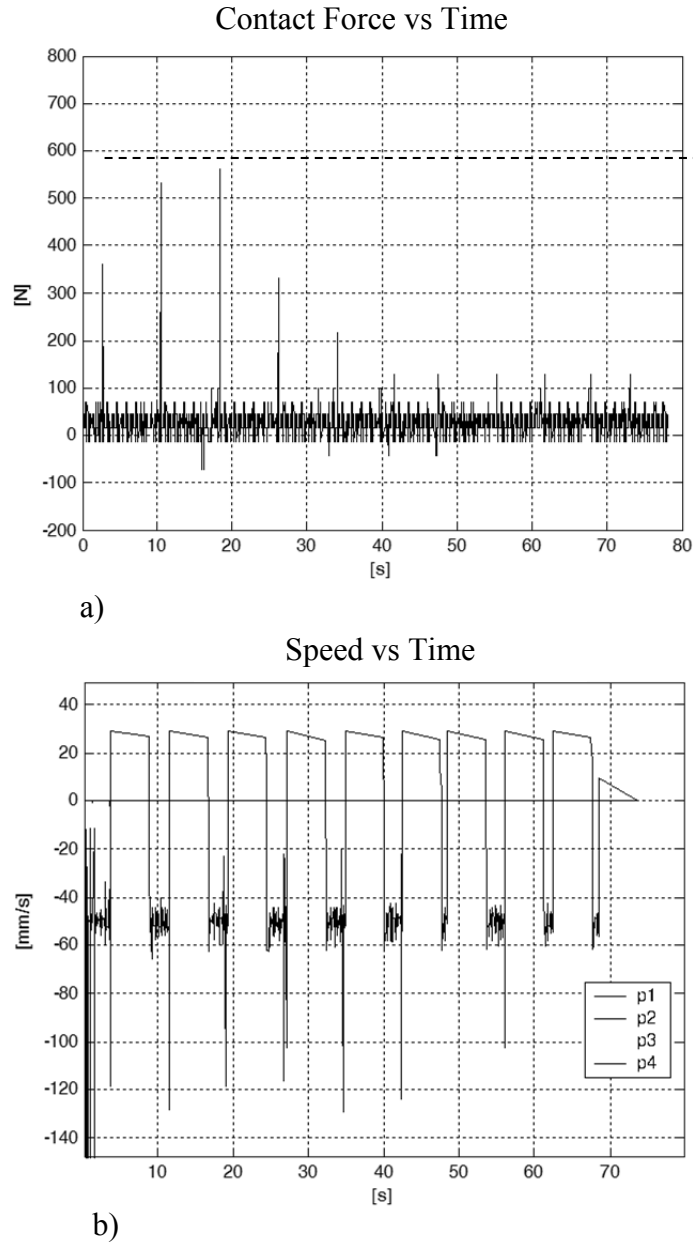## Contact Force vs Time

a)

Speed vs Time

b)

Fig. 13. Force-controlled detection of soil at different leg displacements: a) Force acting on the leg; b) Leg-commanding speed.

Figure 14 uses a graphic sequence to illustrate another experiment. Obstacles of low stiffness were detected, including the hand shown in the last part of the sequence, thus confirming the sensitivity of the built-in force-sensing capability.
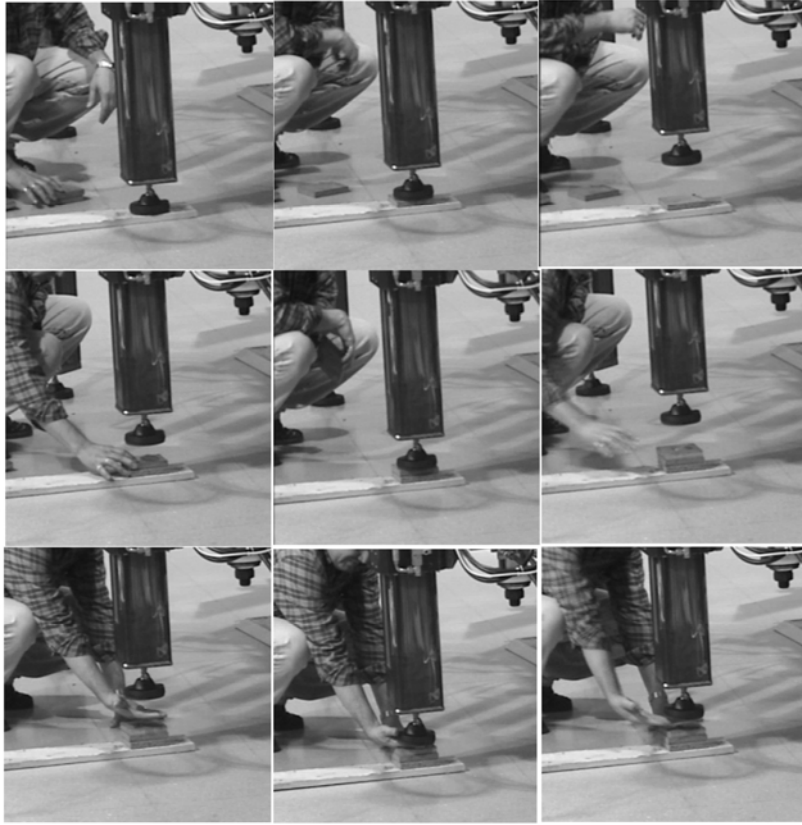
Fig. 14. Graphic sequence showing the force-controlled detection of obstacles.

In another series of experiments, a loose, flexible steel plate was employed to investigate the system's response to low-stiffness soil such as soft ground. In this case, leg 1 of ROBOCLIMBER was used. Figure 15 shows the results of the experiment. The velocity commands were the same as in previous experiments, and the desired force was set at 150 N. In this experiment, it took longer to reach the desired force than in the previous experiment (see Figure 13).   This is because the ground was flexible and presented a degree of compliance with the robot foot, which made the reaction force increase in proportion to the displacement until the requested set point was reached, in contrast to the previous experiments, where the leg was interacting with a soil of greater stiffness. Interestingly, in the case of flexible ground, the commutation happened exactly when the force set point was reached, while in the previous case the forces were much higher (up to three times higher in the experiment shown in Figure 13, except when the travelling distance was very short). This fact can be used to identify the damping characteristics of the ground. Also, when the control system detected the required force and thus made the decision to change the velocity command, the falling edge of the measured force began and completed its decay very quickly, because the leg left contact with the flexible plate faster than the plate could rebound (see Figure 15).
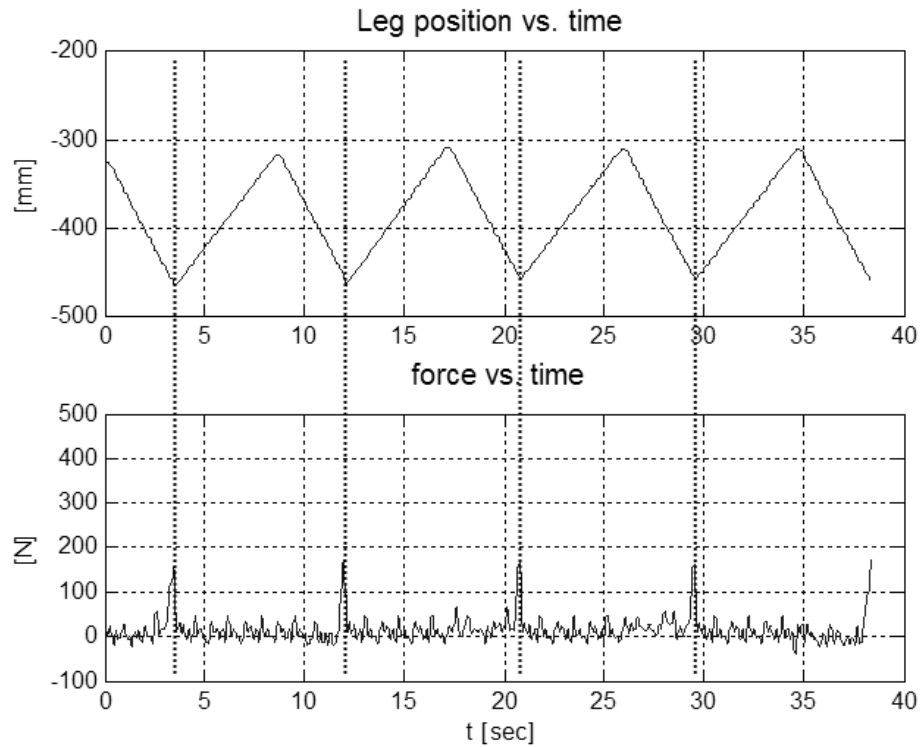
Fig. 15. Position and force data of one leg of ROBOCLIMBER when contacting a flexible steel plate.

Figure 16 is a series of photos showing the movement of the robot leg when it makes contact with the flexible steel plate. Note how the leg remains in contact with the plate during a number of frames, so there is a time delay in the reaction force as compared to the reaction after contact with a stiffer or non-flexible soil.
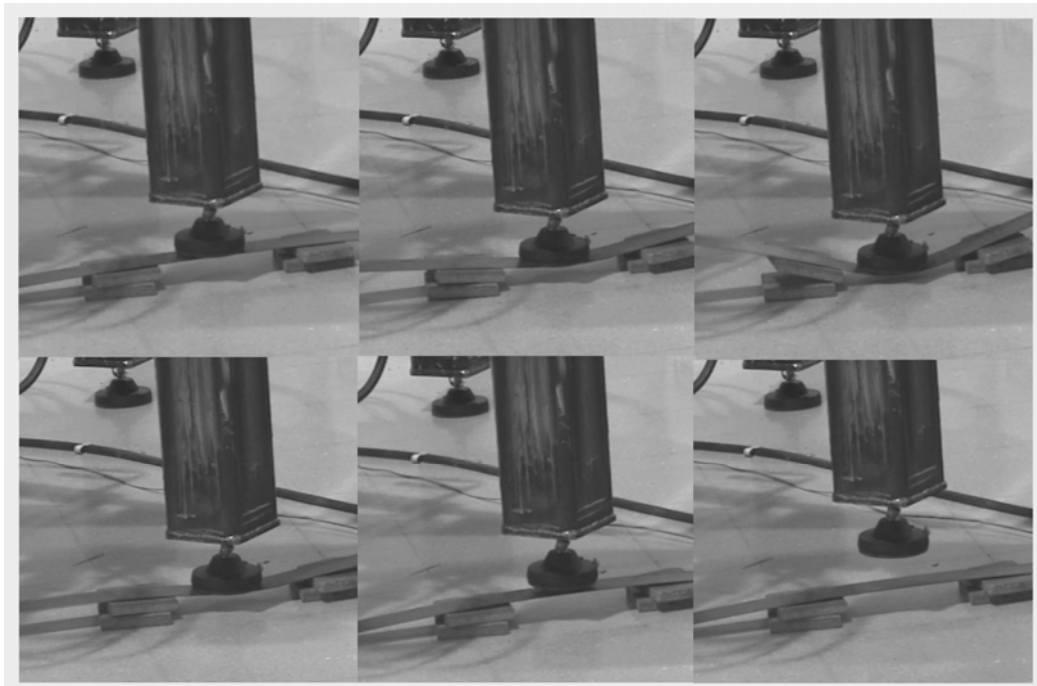

Fig. 16. Sequence showing the interaction of the leg with a flexible steel plate.

When the robot legs interact with compliant or elastic terrain, there is compliant performance. This causes a delay in the measured forces, which depends on ground stiffness. This series of experiments indicates that ROBOCLIMBER's built-in force sensors can detect terrains of different elasticity. Observe that during gait implementation the desired forces will not be so low; in fact, they will be similar to the forces measured in static postures in previous experiments (section 4). Nevertheless, because of the high sensitivity and accuracy of the embedded force sensors, the force sensors can be used in many practical situations.

6. Real-time computation of the zero-moment point for ROBOCLIMBER

Many authors use the concept of the centre of pressure (Orin 1976) and the concept of the zero-moment point (ZMP) to study gait and postural stability in legged (mainly biped) robots, mostly following the pioneering work of Vukobratovic and his co-workers (Vukobratovic and Juricic 1968; Vukobratovic and Stokic 1975; Vukobratovic and Borovac 2004). The ZMP concept is very useful for walking robots, particularly for investigating the force-distribution problem, and we use it herein for our ROBOCLIMBER.

Using the kinematic parameters of ROBOCLIMBER shown earlier in Figure 2, it is possible to obtain the equations for the ZMP of the robot when it is dynamically balanced.

Thus, the ZMP on the sagittal plane is given by

$$ZMP_s = \frac{d_1 \mathbf{a}(\mathbf{Kv} + \mathbf{b}) + \mathbf{cA}(\mathbf{Kv} + \mathbf{b})}{\mathbf{c}(\mathbf{Kv} + \mathbf{b})}$$

(3)

and, on the transversal plane, it can be written as,

$$ZMP_t = \frac{d_2 \mathbf{d}(\mathbf{Kv} + \mathbf{b}) + \mathbf{dB}(\mathbf{Kv} + \mathbf{b})}{\mathbf{c}(\mathbf{Kv} + \mathbf{b})}$$

(4)

where,

$$d_1 = \frac{ls}{2} \quad d_2 = \frac{lf}{2}$$

$$\mathbf{a} = \begin{bmatrix} 1 & 1 & -1 & -1 \end{bmatrix} \quad \mathbf{c} = \begin{bmatrix} 1 & 1 & 1 & 1 \end{bmatrix} \quad \mathbf{d} = \begin{bmatrix} -1 & 1 & -1 & 1 \end{bmatrix}$$

$$\mathbf{b} = \begin{bmatrix} 16.1 \\ 30.0 \\ -33.1 \\ 87.7 \end{bmatrix} \qquad \mathbf{A} = diag.\begin{bmatrix} lp_1 s_1 & lp_2 s_2 & lp_3 s_3 & lp_4 s_4 \end{bmatrix}$$

$$\mathbf{v} = \frac{1}{v_s} \begin{bmatrix} v_{def1} - v_{do1} \\ v_{def2} - v_{do2} \\ v_{def3} - v_{do3} \\ v_{def4} - v_{do4} \end{bmatrix} \qquad \mathbf{B} = diag.\begin{bmatrix} lp_1 c_1 & lp_2 c_2 & lp_3 c_3 & lp_4 c_4 \end{bmatrix}$$

$$\mathbf{K} = diag.\begin{bmatrix} 28651 & 20868 & 23978 & 20463 \end{bmatrix}$$

(5)

Equations (3) and (4) can be used interchangeably to calculate the ZMP if the robot is supported by three or four legs. Any displacement of robot joints is also included in the above expressions.

The ZMP for ROBOCLIMBER was calculated first in a statically stable stance with all four legs of the robot in contact with the ground, forming a quadrilateral shape. The parallelogram measured 2.22 m by 1.84 m. Under these conditions the ZMP was -0.08 m in the sagittal plane and -0.04 m in the lateral plane, with the origin at the geometric centre of the robot. This indicated that the ZMP and the geometric centre lay very close to each other, and this result was in agreement with the previous experiments for calculating ROBOCLIMBER's centre of gravity.

To sense the variations of the ZMP in a statically stable stance under external disturbances, an experiment was conducted consisting in having a person weighing 834 N walk around on top of the robot body. These conditions are relevant to ROBOCLIMBER, because in practice the machine is intended to carry a variable payload. The person's weight was only 4.3% of the robot's full weight; therefore, it was a small disturbance that was expected to give a good indication of how the measurement system (built-in force sensors) performed to detect ZMP displacement in real time. The resulting force measurement was 20110 N (that is, an error of approximately -0.3%); this was the normal force acting on the ZMP (see Figure 17) when the person was moving about on top of the robot.
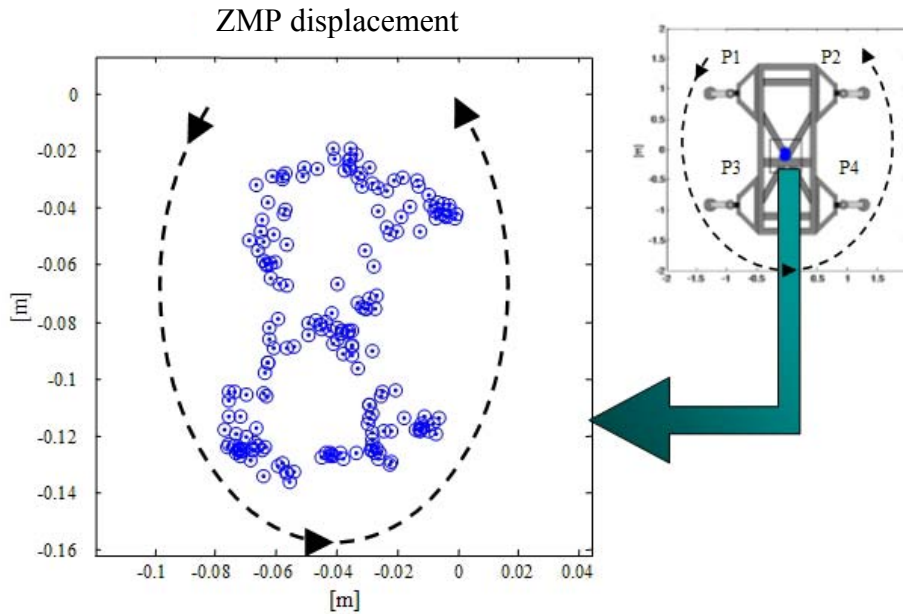

Fig. 17. ZMP variation when a person is walking around on top of the robot.

The person walked anticlockwise from leg 1 to leg 2, and the ZMP registered the same movement. Each measurement (data acquisition, filtering and ZMP computation using (3) and (4)) is made available to the robot control every 50 msec. Maximum variation in this test was 0.117 m in the sagittal ZMP and 0.0768 m in the transversal ZMP.

Several other experiments were carried out in order to measure the ZMP when ROBOCLIMBER was performing a dynamically balanced gait. In these experiments, the robot executed a two-phase discontinuous gait (González de Santos and Jiménez 1995). For illustrating purposes, Figure 18 presents a scheme of the two-phase discontinuous gait for ROBOCLIMBER.
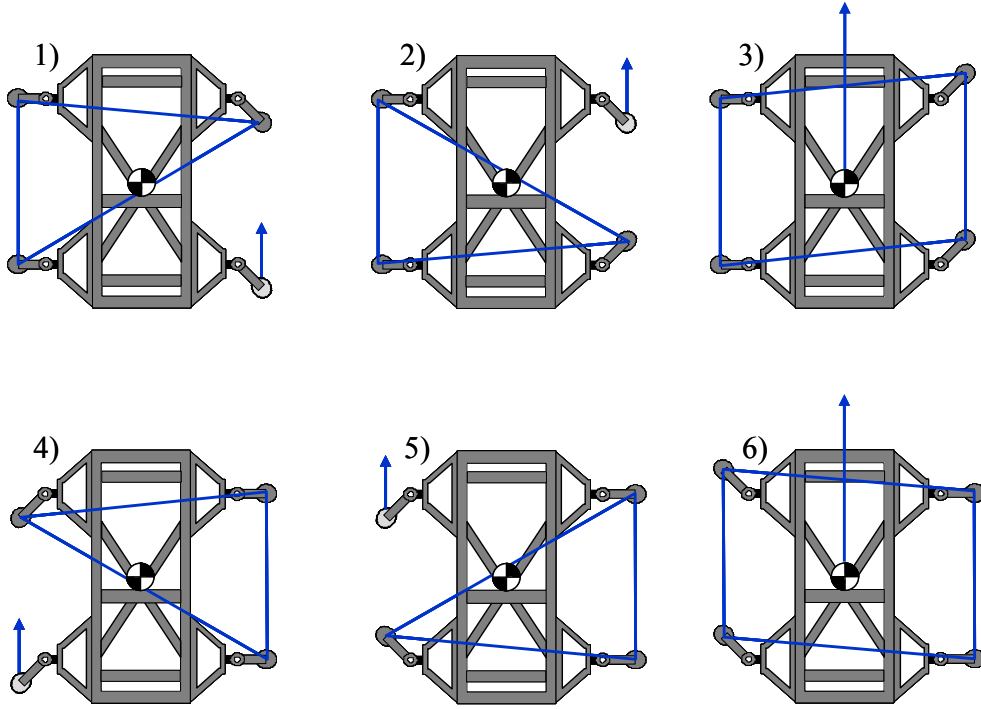

Fig. 18. ROBOCLIMBER: two-phase discontinuous gait.

It was assumed that the vertical axis was the 'z' axis and that this was orthogonal to the robot body as well. In the measurements using the periodic gait, all positions of the 12 DOF's and all vertical leg forces were recorded in real time. In this experiment, the weight of the robot was increased to 21500 N, because a human operator, an autonomous engine to power the robot, and control equipment were added. Figure 19 shows experimental data taken during locomotion on a rigid, flat, horizontal surface.
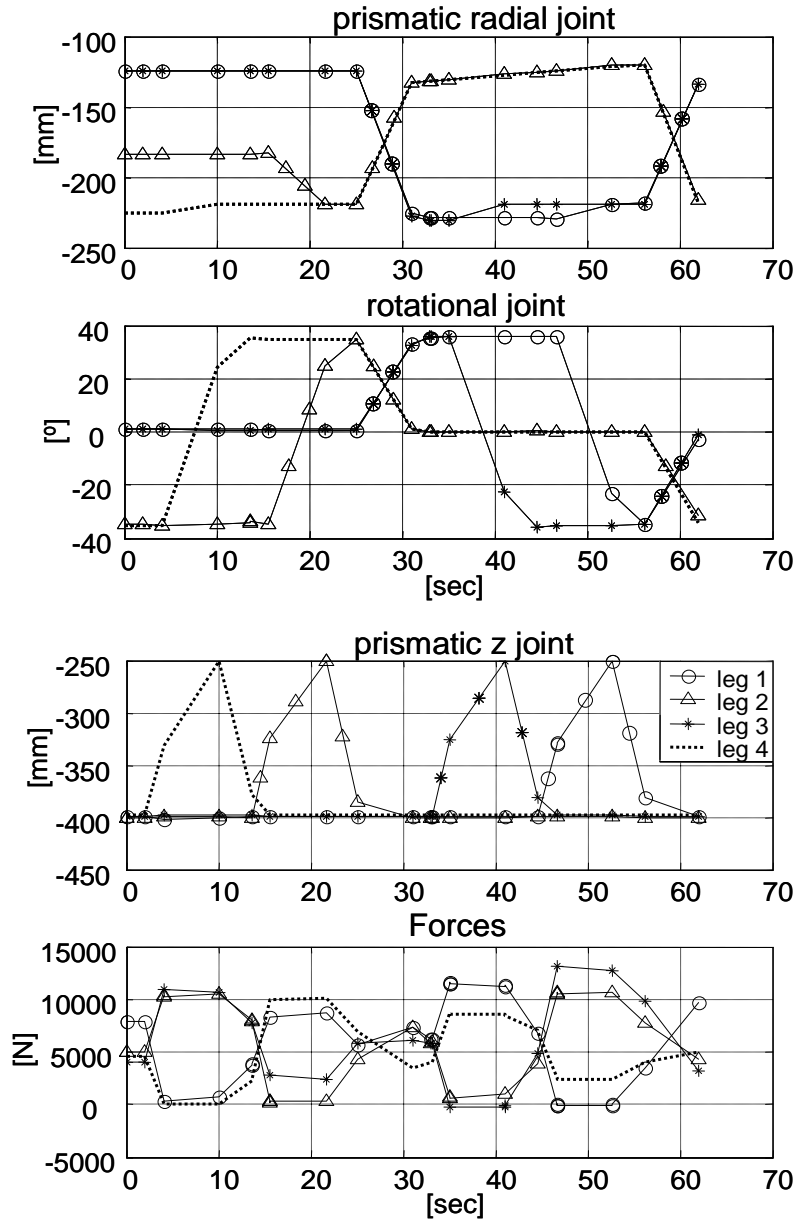
Fig. 19. Measurement of positions and forces in one step of the two-phase discontinuous gait in ROBOCLIMBER.

Interestingly, although the gait is theoretically quasi-static, it is in fact slightly dynamic (see Figure 19). The z-axis positions show that there are instants of time (for example, from 12 to 14 sec and from 44 to 46 sec) when the robot is supported on two legs. This was done as a calculated risk to optimise the gait slightly.

The recorded forces also indicate that, except during the body-motion phase (time 24 sec to 33 sec, approximately), the robot is practically supported on two legs (This is most noticeable during the transfer of leg 4 and leg 3). This was not anticipated and is simply noted here as an experimental observation for which no explanations are offered.
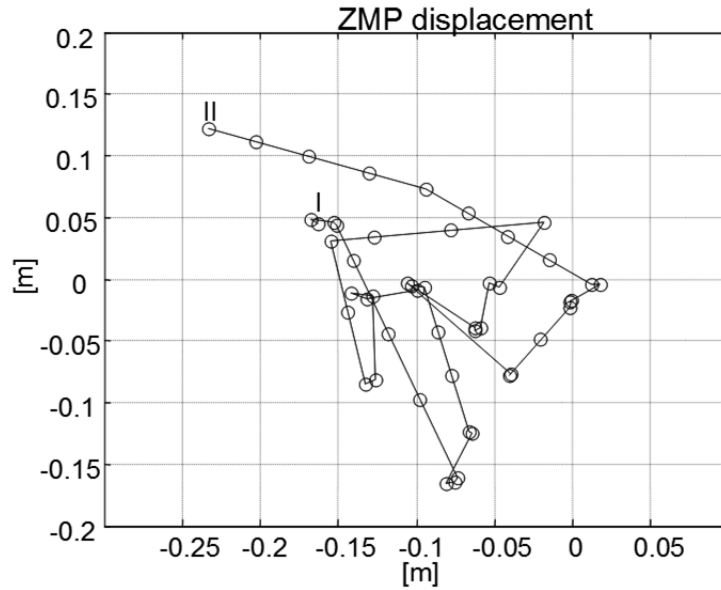
Fig. 20. ZMP computation during a two-phase discontinuous gait in ROBOCLIMBER.

For one step of the robot, the ZMP in the sagittal and transversal planes is calculated using equations (3) and (4), respectively (see Fig. 20). This result demonstrates that the ZMP is inside the support polygon but very near the polygon's boundary. Note that although the gait is "theoretically" symmetric, the ZMP at the start (I in Figure 20) and at the end of the step (II in Figure 20) have different values. This is another fact that reinforces the interest of taking direct measurements.

The average resultant force measurement in this experiment is 22400 N, and it acts at each ZMP during the robot's step. The experimentally observed difference between the stated weight of the machine (21500 N) and the average reaction force (22400 N) during the gait is about 900 N, illustrating the presence of dynamic effects that "increase" the forces involved in contact between the foot and rigid ground. In other words, this fact serves to highlight the advantage of using the ZMP concept for walking robots as an index of dynamic behaviour.

7. Conclusions

This paper looked at force-sensing strategies in legged robots and proposed a methodology for taking account of force-sensing requirements at the robot's design stage, with a view to embedding force-sensing capability within the robot's mechanical structure. Using the full mechanical configuration of ROBOCLIMBER, a bulky climbing and walking machine, a finite-element analysis of the mechanical structure of the robot legs was performed and specific positions for strain gages were selected to measure indirectly the contact forces between the feet and the ground. After the sensors were calibrated, they were employed to compute the centre of gravity for ROBOCLIMBER and proved useful for determining COG variation during a gait (due to the non-negligible weight of the robot's legs). A simple control algorithm was employed to control foot-soil interaction for soils with different stiffness properties. The paper also showed how built-in force sensors can be used to measure the ground reaction forces and to compute the ZMP for ROBOCLIMBER in real time, both while standing, in order to ascertain the point where the reaction force of the ground acts, and while executing a dynamically balanced gait. Several interesting results of the experiments were indicated.

Acknowledgements

References

Acaccia G., Bruzzone L. E., Michelini R. C., Molfino R. M., and Razzoli R. P. 2000. A tethered climbing robot for firming up high-steepness rocky walls. In *Proc. of the 6th Intl. Conf. on Intelligent Autonomous Systems (IAS)*, Venice, Italy.

Anthoine P., Armada M., Carosio S., Comacchio P., Cepolina F., González P., Klopf T., Martin F., Michelini R. C., Molfino R. M., Nabulsi S., Razzoli R. P., Rizzi E., Steinicke L., Zannini R., and Zoppi M. 2003. ROBOCLIMBER. In *International Workshop on Advances in Service Robotics*, Bardolino, Italy.

Arikawa, K. and S. Hirose, S. 1996. Development of quadruped walking robot TITAN VIII. In *Proc. International Conference on Intelligent Robots and Systems* 1: 208-214.

Armada, M. 1991. Telepresence and Intelligent Control for a Legged Locomotion Robot. *Expert Systems and Robotics,* Springer Verlag, pp. 377-396.

Armada, M. 2000. Climbing and walking: from research to applications. In *Proceedings of 3rd International Conference on Climbing and Walking Robots*, Madrid, Spain, pp. 39-48.

Armada, M. and González de Santos, P. 1997. Climbing, walking and intervention robots. *Industrial Robot* 24 (2): 158-163.

Armada, M., Maza, M., González de Santos, P., Fontaine, J.G., and Papantoniou, V. 1997. Tracminer: Traction enhancement mining equipment accessory. *Industrial Robot* 24 (5): 370-375.

Armada, M., and González de Santos, P. 2001. Perspectives of climbing and walking robots for the construction industry. In *Proceedings of the 4th International Conf. on Climbing and Walking Robots*, Paris, France, pp. 929-936.

Armada, M., González de Santos, P., and Prieto, M. 2002. Climbing and Walking Robots for the Petrochemical Industry and for Underwater Applications. In *Proceedings of the 5th International Conf. on Climbing and Walking Robots*, Paris, France, pp. 939-946.

Armada M., and Molfino R M. 2002. Improving Working Conditions and Safety for Landslide Consolidation and Monitoring. In *Proc. Workshop on the role of CLAWAR in education, training, working conditions and safety*, Madrid, Spain.

Armada, M., González de Santos, P., Jiménez, M.A. and Prieto, M. 2003. Application of CLAWAR machines. *International Journal of Robotics Research*, 22(3-4):251-264.

Bentley, J. P. 1995. Principles of Measurement Systems, *3rd ed., Pearson Education Limited*, Harlow, England.

Carelli, R., Oliva, E., Soria, C., and Nasisi, O. 2004. Combined force and visual control of an industrial robot. *Robotica*, (22):163-171.

Chiaverini, S., and Siciliano, B. 1999. A survey of robot interaction control schemes with experimental comparison. *Journal of IEEE/ASME Transactions on Mechatronics*, 4(3): 273-285.

Dally, J. W., Riley, W. F., and McConnell, K. G. 1993. Instrumentation for Engineering Measurements. *Wiley, Singapore*.

De Schutter, J., Bruyninckx, H., Zhu, W. H., and Spong, M.W. 1998. Force control: A bird's eye view. In *Control Problems in Robotics and Automation*, Springer-Verlag, London, pp. 1-17.

Discovery Channel 2005. Roboclimber Project Report. In *Daily Planet Archive* available at http://www.exn.ca/dailyplanet/view.asp?date=1/21/2005.

Estremera, J. and González de Santos, P. 2003. Free gaits for quadruped robots over irregular terrain. *The International Journal of Robotics Research* 22(2):115-130.

Fisher, W. D., and Mujtaba, M. S. 1992. Hybrid Position/Force Control: A Correct Formulation. *The International Journal of Robotics Research*, 11(4): 299-311.

Gálvez J. A., González de Santos P., and Armada M. 1998. A Force Controlled Robot for agile Walking on Rough Terrain. In *Proc. ICV'98*, Sevilla, Spain.

Galvez, J.A., Estremera, J. and Gonzalez de Santos, P., 2000. SILO4-a versatile quadruped robot for research in force distribution. In *Proceedings of 3rd International Conference on Climbing and Walking Robots*, Madrid, Spain, pp. 371-383.

Gardner, J. F. 1992. Efficient Computation of Force Distributions for Walking Vehicles on Rough Terrain, *Robotica,* 10: 427-433.

González de Santos, P., Armada, M., Martin, A., and de Peuter, W. 1994. A survey of locomotion concepts for planetary exploration rovers. In *Proceedings of 3rd ESA Workshop on Advance Space Technologies for Robot Applications,* Noordwjck, Netherlands.

Gonzalez de Santos, P., and Jimenez, M. A. 1995. Generation of Discontinuous Gaits for Quadruped Walking Vehicles. *Journal of Robotic Systems*, 12(9): 599-611.

González de Santos, P., Armada, M., and Jiménez, M.A. 2000. Ship building with ROWER. *IEEE Robotics and Automation Magazine*. 7(4):35-43.

Gorinevsky, D. M., and Schneider, A. Y. 1990. Force Control in Locomotion of Legged Vehicles over Rigid and Soft Surfaces. *The International Journal of Robotics Research* 9(2): 4-23.

Gorinevsky, D. M., Formalsky, A. M., and Schneider, A. Y. 1997. Force Control and Robotics Systems. *CRC Press*.

Grieco, J. C., Armada, M., Fernández, G., and González de Santos, P. 1994. A review on force control of robot manipulators. *Studies in Informatics and Control* 3:241-252.

Grieco, J.C., Prieto, M., Armada, M. and González de Santos, P. 1998. A six-legged climbing robot for high payloads. In *Proceedings of the IEEE International Conference on Control Applications*, Trieste, pp. 446-450.

Hirose, S. 1997. TITAN VII: Quadruped Walking and Manipulating Robot on a Steep Slope. In *Proceedings of the IEEE International Conference on Robotics and Automation*, Albuquerque.

Hogan, N. 1985. Impedance control: an approach to manipulation. *J Dynamic Systems, Measurement, and Control* 107:1-24.

Kumar V., and Waldron K. J. 1990. Force Distribution in Walking Vehicles. *Journal of Mechanical Design* 112:90-99.

Maza, M., Fontaine, J.G., Armada, M.A., González, P., Papantoniou, V., and Mas, M. 1997. Wheel+legs- A new solution for traction anhancement without additive soil compaction. IEEE *Robotics&Automation Magazine* 4(4):26-33.

Molfino, R.M., Armada, M., Cepolina, F., and Zoppi, M. 2005. Roboclimber the 3 ton spider. Industrial Robot 32(2):163-170.

Mosher, R. S. 1968. Test and Evaluation of a Versatile Walking Truck. In *Proceedings of Off-Road Mobility Research Symposium*, International Society for Terrain Vehicle Systems, Washington D.C., pp. 359-379.

Montes, H., Nabulsi, S., Armada, M., and Sanchez V. 2004. Design and Implementation of Force Sensor for Roboclimber. In *Proceedings of the 7th International Conf. on Climbing and Walking Robots*, Madrid, Spain, pp. 219-227.

Montes, H., Nabulsi, S., and Armada, M. 2004a. Detecting Zero-Moment Point in legged robot. In *Proceedings of the 7th International Conf. on Climbing and Walking Robots*, Madrid, Spain, pp. 229-236.

Montes, H. 2005. Análisis, diseño y evaluación de estrategias de control de fuerza en robots caminantes. *Ph.D. Thesis*, Univ. Complutense de Madrid, Spain.

Nabulsi, S., Armada, M., and González de Santos, P. 2003. Control Architecture for a Four-Legged Hydraulically Actuated Robot. In *Proc. of Measurement and Control in Robotics* (ISMCR'03), Madrid, Sapin, pp. 291-295.

Nabulsi, S., and Armada, M. 2004. Climbing Strategies for Remote Maneuverability of ROBOCLIMBER. In *Proc. of the 35th International Symposium on Robotics,* Paris, France.

Nabulsi, S., Montes, H., and Armada, M. 2004. ROBOCLIMBER: control system architecture. In *Proceedings of 7th International Conference on Climbing and Walking Robots*, September 22-24, Madrid, Spain.

Orin, D.E. 1976. Interactive control of a six-legged vehicle with optimization of both stability and energy. *Ph.D. Thesis*. The Ohio State University.

Pfeiffer, F., Löffler, K. and Gienger, M. 2000. Design Aspects of Walking Machines. In *Proc. 3rd International Conf. on Climbing and Walking Robots*, Madrid, pp. 17-38.

Pugh, D.R., Ribble E.A., Vohnout V.J., Bihari, T.E., Walliser, T.M., Patterson, M.R., and Waldron, K.J. 1990. Technical Description of the Adaptive Suspension Vehicle. *International Journal of Robotics Research* 9(2): 24-42.

Salisbury J. K., and Roth B. 1983. Kinematic and force analysis of articulated mechanical hands. *J. of Mechanisms, Transmissions and Automation Design* 105:35-41

Siciliano B., and Villani L. 1999. Robot Force Control. *Kluwer Academy Publishers*, Norwell, Massachusetts.

Song, S.M. and Waldron, K.J. 1988. Machines That Walk: The Adaptive Suspension Vehicle. *MIT Press*.

Spong M., and Vidyasagar M 1989. Robot Dynamics and Control. *John Wiley & Sons*. Singapore.

Steinicke, L., Dal Zot, C. and Benoist, T. 2004. A system for monitoring and controlling a climbing and walking robot for landslide consolidation. In *Proc. IARP Workshop on Robotics and Mechanical Assistance in Humanitarian Demining and Similar Risky Interventions*, Brussels, Belgium.

Virk, G.S., Muscato, G., Semerano, A., Armada, M., and Warren, H.A. 2004. The CLAWAR project on mobile robotics. *Industrial Robot*, 31(2):130-138.

Vukobratovic, M. and Juricic, D. 1968. Contribution to the synthesis of biped gait. In Proc. *IFAC Symp. Technical and Biological Problem on Control*, Erevan, USSR.

Vukobratovic, M. and Stokic, D.1975. Dynamic Control of Unstable Locomotion Robots. *Mathematical Biosciences*, 24:129-157.

Vukobratovic, M. and Borovac, B., 2004. Zero-Moment Point – Thirty Five Years of its Life. *International Journal of Humanoid Robotics*, 1(1):157:173.

Waldron, K.J., and Kinzel, G.L. 1999. Kinematics, dynamics and design of machinery. John Wiley & Sons.

Waldron, K.J. 2000. From walking to galloping. In Proc 3rd *Int. Conference on Climbing and Walking Robots*. Professional Engineering Publishing, Madrid, Spain, pp. 1-5.

Whitney, D. E. 1987. Historical perspective and state of the art in robot force control. *The International journal of Robotic Research* 6(1):3-14

LIST OF FIGURE CAPTIONS

Fig.1. Kinematic parameters of ROBOCLIMBER; (a) Top view of the robot; (b) lateral view of one leg; (c) 3D view showing main dimensions (in mm.).

Fig.2. ROBOCLIMBER working on a slope. Only some acting forces are shown: f_t: tensioning force; f_p: propulsion force; f_s: support force; f_d: drilling force. ROBOCLIMBER design courtesy of PMARLab (University of Genoa).

Fig. 3. ROBOCLIMBER field tests: a) Climbing: Alps, Northern Italy; b) Walking: Industrial Automation Institute (IAI-CSIC) outdoor facilities.

Fig. 4. Force analysis on the leg of ROBOCLIMBER: a) Scheme of force distribution; b) FEA on the leg structure; and, c) FEA on the foot.

Fig. 5. (a) ROBOCLIMBER's leg made of steel of different kinds; (b) force sensor at the top of the leg; (c) force sensor on the side beam of the leg; and (d) force sensor on the support axis of the foot.

Fig. 6. Calibration results and comparison between two different force-sensor configurations.

Fig. 7. Force measurement with the leg top sensors.

Fig. 8. Force measurement with the sensors on the support axis of the foot.

Fig. 9. Centre of gravity of ROBOCLIMBER.

Fig. 10. Using force sensors to find how ROBOCLIMBER's centre of gravity changes during a gait cycle.

Fig. 11. Controlling foot-ground interaction using simple force feedback.

Fig. 12. Force-controlled detection of ground at different heights. In this experiment, leg length ranged from 0 (retracted) to 500 mm (less than maximum possible extension). The force set point was 150 N.

Fig. 13. Force-controlled detection of soil at different leg displacements: a) Force acting on the leg; b) Leg-commanding speed.

Fig. 14. Graphic sequence showing the force-controlled detection of obstacles.

Fig. 15. Position and force data of one leg of ROBOCLIMBER when contacting a flexible steel plate.

Fig. 16. Sequence showing the interaction of the leg with a flexible steel plate.

Fig. 17. ZMP variation when a person is walking around on top of the robot.

Fig. 18. ROBOCLIMBER: two-phase discontinuous gait.

Fig. 19. Measurement of positions and forces in one step of the two-phase discontinuous gait in ROBOCLIMBER.

Fig. 20. ZMP computation during a two-phase discontinuous gait in ROBOCLIMBER.